RSC Advances

Ag-mesh-combined graphene for an indium-free current spreading layer in near-ultraviolet light-emitting diodes

Journal:	*RSC Advances*
Manuscript ID:	RA-ART-06-2015-012642.R1
Article Type:	Paper
Date Submitted by the Author:	13-Aug-2015
Complete List of Authors:	Min, Jung-Hong; Gwang-ju Institute of Science and Technology (GIST), Jang, So-Yeong; Gwang-ju Institute of Science and Technology (GIST), Kim, Ki-Young; Gwang-ju Institute of Science and Technology (GIST), Choi, Sang-Bae; Gwangju Institute of Science and Technology, School of Information and Communications Seong, Won-Seok; Gwang-ju Institute of Science and Technology (GIST), Lee, Dong-Seon; Gwangju Institute of Science and Technology, School of Information and Communications

Ag-mesh-combined graphene for an indium-free current spreading layer in near-ultraviolet light-emitting diodes

Jung-Hong Min,[1, 2] So-Yeong Jang,[1, 2] Ki-Young Kim,[1, 2] Sang-Bae Choi,[1, 2] Won-Seok Seong,[1, 2] and Dong-Seon Lee[1, 2, *]

[1]School of Information and Communications, Gwangju Institute of Science and Technology, Gwangju 500-712, Korea

[2]Research Institute for Solar and Sustainable Energies, Gwangju 500-712, Korea

Corresponding Author

* dslee66@gist.ac.kr

Abstract

We have designed and fabricated Ag-mesh-combined graphene current spreading layers (CSLs) for GaN-based near-ultraviolet light-emitting diodes (NUV LEDs). Three different types of the CSLs were fabricated having 300 μm, 150 μm, and 75 μm gaps between the mesh lines. Optical and electrical properties were investigated and the performance of the LEDs having the CSLs and were compared with those of LEDs having indium tin oxide and graphene CSLs. The light output power of the LEDs with the Ag-mesh-combined graphene CSL adopting 150 μm-gap was highest at both the same current injection and at the same input power. This was possible due to the lowering of the sheet resistance via the adoption of an Ag mesh and the networking of the Ag mesh using a graphene sheet with very little transmittance loss.

1. Introduction

Near-ultraviolet light-emitting diodes (NUV LEDs) are currently used in a wide-range of technologies such as bio, medical, and illumination engineering [1-3]. For these NUV LED applications, better extraction of the light via the use of proper current spreading layers (CSLs), which extraction is as important as the proper growth of the epilayer, strongly improves the optical output power of lateral NUV LEDs by decreasing current crowding and improving the efficiency droop [4, 5]; thus, it is essential to utilize proper CSLs in lateral NUV LEDs. Due to its high transparency, low sheet resistance, and suitable contact property, indium tin oxide (ITO) has commonly been used for CSLs in lateral NUV LEDs as well as in visible LEDs. However, a large amount of indium, well known as one of the rare elements, is used not only for transparent conductive oxides but also for optoelectronic devices such as InGaN-based LEDs and CIGS solar cells, which results in price increases of indium [6, 7]. Accordingly, for CSL applications, many attempts have been made to replace indium with graphene, metal nanowires, or thin metal layers [8-13]. Among all these alternative CSLs, graphene has many advantages such as outstanding transparency and conductivity, and mechanical and chemical stability [14-16]. In particular, while the transparency of ITO dramatically decreases due to absorption when approaching the wavelength of ~310 nm, which corresponds to the bandgap of ITO (4 eV) [17], graphene continuously maintains high transparency [8, 18]. However, we found that graphene alone is unstable and eventually leads to failure during operation, as reported previously, because of its high sheet resistance and low work function [19]. Also, while metal nanowires and thin metal layers can considerably improve the electrical properties, the optical properties such as the transparency are not good enough for CSL applications [9-12].

In contrast to metal nanowires and thin metal layers, metal mesh can be used to simultaneously achieve low sheet resistance and high transparency with a proper design using line width, height, and gaps among the lines [20-24]. However, although metal mesh alone can greatly reduce the resistance and improve the electrical properties, it does not provide sufficient current spreading because the current only flows along the metal lines. For better current spreading, an additional material having a sheet shape is required; graphene is a good candidate material since it has a two dimensional sheet shape, a good electrical property, and high transparency. Furthermore, we have constructed an additional supporting layer beneath a *p*-metal pad in our metal mesh. The supporting layer has contributed to outstanding contact properties of the LED devices by stabilizing current flow from the *p*-metal pad.

In this work, due to its high conductivity and good stability, we adopted Ag metal mesh and a graphene sheet grown by chemical vapor deposition (CVD). We used microscale Ag mesh, for the following reasons: (i) compared to nanoscale metal mesh, microscale Ag mesh can be easily fabricated by conventional photolithography; (ii) using conventional photolithography, the Ag-mesh combined graphene CSL can be immediately used in practical optoelectronic industries; (iii) fabrication of microscale Ag mesh is very stable.

Herein, to identify the usefulness of Ag mesh for CSLs in NUV LEDs, of which the peak wavelength is ~380 nm, we have fabricated Ag-mesh-combined graphene CSLs having three different types of gap (300 μm, 150 μm, and 75 μm), with 5 μm width and 200 nm height. Furthermore, instead of the rectangular shapes used for LEDs, we have designed radial shapes for the Ag mesh because the rectangular shapes, having two electrodes placed diagonally, were not likely to be suitable or efficient in our device structure. With low sheet resistance and moderate transmittance, the LEDs with 150 μm-gap radial Ag mesh on graphene CSLs showed the best improvement in light output power—up to 34.4% compared

to that of 200 nm-thick ITO CSLs for 50 mA current injection. Thus, we were able to fabricate effective CSLs in NUV LEDs by taking good advantage of both Ag mesh and graphene; as well, we assumed that the CSLs, which combine metal mesh and graphene, can be easily operated in visible LEDs.

2. Experimental section

2. 1. Fabrication process of LED devices

Figure 1 shows the process flow of the fabrication of NUV LEDs having 400 μm × 400 μm dimension with five types of CSLs, namely: 200 nm-thick ITO (ITO), graphene only (GR), 300 μm-gap radial Ag mesh on graphene (RAM 300), 150 μm-gap radial Ag mesh on graphene (RAM 150), and 75 μm-gap radial Ag mesh on graphene (RAM 75). The NUV LEDs consist of *p*-GaN/Multi-quantum wells (MQWs)/*n*-GaN/un-doped GaN/sapphire substrate; the mesa structures were fabricated by photo-lithography and inductive coupled plasma etching. On the base of the mesa structures, ITO patterns were formed using a negative photoresist (PR); deposition of the 200 nm-thick ITO was done using e-beam evaporation. Then, the PR was removed and the ITO layer was annealed by rapid thermal annealing at 600 ºC in air ambient for 5 minutes. Graphene grown on a copper foil by CVD was transferred to the mesa structures of GR, RAM 300, RAM 150, and RAM 75. The detailed graphene transfer process followed that of our previous method [19]. We performed graphene patterning on the transferred graphene for GR using positive PR and etched the graphene using O_2 plasma in a reactive ion etching (RIE) process. The rest of the PR on the graphene was removed by acetone and weak-air spray acetone. For RAM 300, RAM 150, and RAM 75, we formed the radial mesh patterns by conventional photolithography using negative PR. After the deposition of 200 nm-thick Ag onto the transferred graphene via e-beam evaporation, the PR was stripped by acetone and weak-air spray acetone. The rest of the

graphene sheet, except that beneath the radial metal mesh, was etched using O_2 plasma with a PR mask. The NUV LEDs with five different types of CSLs were completed by simultaneously deposition of *p*- and *n*- metal pads (Cr/Au) using e-beam evaporation.

2. 2. Thickness variation of Ag mesh

We have transferred the graphene sheets on the sapphire substrates and formed the Ag mesh by increasing the thickness of the Ag mesh from 5 nm to 200 nm by photolithography and e-beam evaporation. The sheet charge density and mobility values of the Ag-mesh-combined graphene sheet having different thickness of Ag were measured by Hall measurement. Hall measurement was conducted with the indium balls deposited on the 4 corners of the square sapphire substrates fully covered with Ag-mesh-combined graphene sheets.

3. Results and discussion

To examine the electrical and optical properties, we also prepared five types of CSLs on the double-polished sapphire (DPS) substrates. As can be seen in Fig. 2(a), optical microscope images of the CSLs prepared on DPS clearly show well-made CSLs fabricated through a conventional photolithography process. In order to verify the existence of graphene on DPS, we performed Raman spectroscopy. Figure 2(b) shows the clear G peaks and 2D peaks of the graphene sheet transferred to DPS (GR), the 300 μm-gap Ag mesh on graphene (Mesh 300), the 150 μm-gap Ag mesh on graphene (Mesh 150), and the 75 μm-gap Ag mesh (Mesh 75). The sheet resistances of the CSLs were obtained by Hall measurement, with results shown in Fig. 2(c). The sheet resistances of the 200 nm-thick ITO and the graphene sheet were 26.1 Ω/□ and 706 Ω/□, respectively, which values are comparable to those we previously obtained for ITO (39 Ω/□ for 150 nm thick) and graphene (739 Ω/□) [19]. The sheet resistance of the graphene alone was so high that the material is very likely to be unstable when it is used as a

CSL. By comparison, when the graphene sheet was combined with the Ag mesh, much lower sheet resistances were observed, with values of 6.2 Ω/□ for Mesh 300, 2.3 Ω/□ for Mesh 150, and 1.4 Ω/□ for Mesh 75. Thus, the Ag mesh did dramatically reduce the sheet resistances of the graphene sheet. While the sheet resistance of the graphene sheet alone was high, the transmittance was the highest, 95.1 %, at 380 nm, as shown in Fig. 2(d). Even when graphene was combined with Ag mesh, it was possible to maintain the transmittance of graphene at a level high enough for the material to be used as a CSL. The transmittances of Mesh 300, Mesh 150, and Mesh 75 were 91 %, 86.2 %, and 76.2 %, respectively, at 380 nm. The transmittances of Mesh 300 and Mesh 150 turned out to be lower than those of ITO (92.7 % at 380 nm) and graphene (95.1 % at 380 nm) but still high enough for these materials to be used as CSLs [25]. However, the transmittance of Mesh 75 was not high enough for this material to be used as a CSL; the low transmittance is due most likely to a shading of the surface area by the Ag mesh. Transmittance was estimated for RAM 300, RAM 150, and RAM 75 according to the following equation:

$$T_{Calculated}(\%) = 100 \times (1 - \frac{A_{Mesh}}{A_{MQW}}) \quad (1)$$

where A_{Mesh} and A_{MQW} are the area of the Ag mesh and the MQW, respectively. From the radial mesh design shown in Fig. 2(e), we were able to obtain the ratio of the area of the Ag mesh to that of MQW; this ratio is shown as the red-dotted lines. The calculated transmittances were 84.6 %, 81.3 %, and 73% for RAM 300, RAM 150, and RAM 75; these values are lower than those obtained from the rectangular Ag mesh. The discrepancy is due to the opaque *p*-metal pad of the radial mesh in the LEDs, which was not included in the rectangular Ag mesh. Thus, we confirmed that the transmittance of the radial Ag-mesh-

combined graphene CSLs showed the same trend as that of the rectangular Ag-mesh-combined graphene CSLs, as shown in Fig. 2(f).

As can be seen from the slope of the I-V curves of the NUV LEDs, which become gradually precipitous, as shown in Fig. 3(a), from GR to RAM 75, the series resistance values decrease due to the decrease of the sheet resistance, which results from the adoption of the radial Ag mesh. The series resistance values of GR, RAM 300, RAM 150, and RAM 75 were 122 Ω, 41.3 Ω, 40.4 Ω, and 32.9 Ω, respectively. Despite the sufficiently reduced series resistance values, the turn-on voltage values at 20 mA of the radial Ag mesh CSLs (5.7 V for RAM 300, 5.1 V for RAM 150, and 5 V for RAM 75) were still higher than that of ITO (4.3 V). The elevated turn-on voltage is thought to originate partly from the work function of graphene (4.49 eV), which is lower than that of ITO (4.7 eV), and which gives rise to a high contact resistance between the Ag mesh and *p*-GaN, leading to a high turn-on voltage. The work function values of ITO and graphene were measured by ultraviolet photoelectron spectroscopy [19]. Figure 3(b) shows that all the LEDs with various CSLs emit ultraviolet light at a wavelength of around 380 nm. Light output power was measured for all LEDs with various CSLs and was plotted vs. current [Fig. 3(c)] and vs. input power [Fig. 3(d)]. As can be seen in Fig. 3(c), the LEDs with the graphene CSL only (GR) showed unstable light emission and eventually died even with a current injection below 30 mA; this instability resulted from the high sheet resistance and low work function of the graphene, as was seen in the previous results [19]. On the other hand, the light output power of the LEDs with RAM 150 was the highest at both the same current injection and the same input power. The light output power of the LED using RAM 150 was even higher than that of the LED using ITO, with a value of up to 34.4 % at 50 mA and 14.2 % at the same input power, as can be seen in Figs. 3(c) and 3(d). The light output power of RAM 300 was higher than that of ITO at the

same current injection but was lower at the same electrical input power. This lower power efficiency of the RAM 300 can be explained by its relatively higher resistance and turn-on voltage. In the case of RAM 75, the light output power was the lowest at both the same current injection and at the same input power due to the very low transparency. We are certain that the main reason for RAM 150 showing the highest light output power is the better current spreading through the Ag mesh and the networking of each line of the Ag mesh via a graphene layer, which leads to very little transparency loss.

In order to investigate the current spreading, we injected current through tungsten tips to the *p*- and *n*-metal pads, as can be seen in Fig. 4(a). Because it is hard to observe graphene by optical microscopy, we also measured the Raman spectra of all the LEDs to make sure of the existence of the transferred graphene on the LEDs; Raman results can be seen in Fig. 4(c). The G peaks and 2D peaks of graphene can be clearly seen in the NUV LEDs with GR, RAM 300, RAM 150, and RAM 75. Figure 4(b) shows the images of light emission of each LED at 20 mA injection. We were able to visualize how uniform the light emission is for RAM 300, RAM 150, and RAM 75, especially in comparison with that for GR. In order to identify the uniformity of the light intensity over the distance, we used the image processing function of MatLab and measured the light intensity from the p-metal pad to the n-metal pad, indicated by the white-color dotted arrows that can be seen in Fig. 4(b). In the case of GR, when measured at 20 mA from the *p*-metal pad to a 150 μm distance, the light intensity was higher near the opaque p-metal pad than in the other light emitting regions. This high light intensity of GR at the *p*-metal pad results from current crowding due to the high sheet resistance and the low work function of graphene. Consequently, the light intensity was found to dramatically decrease in the rest of the regions away from the *p*-metal pad. The current spreading of the RAM 300 CSL is better than that of the GR CSL, as shown in Fig. 4(d), but

still not as good as that of ITO CSL, due most likely to the wide gap of the metal mesh. Although RAM 75, because it had the lowest sheet resistance, showed the most uniform emission over the whole light emitting region, it had the lower overall light output power because this sample has the lowest light emission area. We confirmed that the highest light output power of the NUV LEDs was obtained using RAM 150; the high output resulted from the enhanced current spreading due to the low sheet resistance and networking of the Ag mesh with the graphene layer; as a result, RAM 150 has a proper transparency level in comparison with those of RAM 300, RAM 75, and ITO.

In order to verify the origin of the outstanding current spreading for Ag-mesh-combined graphene, we fabricated Ag mesh on graphene by increasing the thickness of the Ag mesh with a 150 μm gap and 5 μm line width and measured the sheet resistance, sheet charge density, and mobility values as shown in Fig. 5(a) and 5(b). The sheet resistance is obtained using the following equation:

$$R_{sh} = \frac{1}{\mu N_s} \quad (2)$$

where R_{sh} is the sheet resistance and μ and N_s are the major carrier mobility and the surface charge density. According to the equation, the sheet resistance value is determined by the mobility and the surface charge density of the material. As can be seen in Fig. 5(b), the sheet resistance of a pristine graphene sheet was very high due to the low surface charge density, in spite of the very high mobility. However, the sheet resistance value of the pristine graphene sheet combined with Ag mesh sharply decreased with an increase of the Ag mesh thickness on the graphene sheet. Although the mobility of Ag-mesh-combined graphene decreases with increasing of the thickness of the Ag mesh, the surface charge density increases exponentially, more than compensating for the decrease of the mobility. Thus, the main reason for the

reduced sheet resistance with respect to the Ag-mesh-combined graphene is the rapid increase of the surface charge density due to the increase of the thickness of the Ag mesh; this situation is very similar to the doping effect in semiconductors [26]. As a result, lateral current in the LED using RAM 150 CSL flows much more uniformly along the Ag mesh lines and the graphene sheet compared to the cases of ITO and GR CSL, as shown in Fig. 5(c).

In order to study the current distribution more accurately, we simulated the lateral current distribution through ITO, GR, and RAM 150 CSL in the LEDs by using COMSOL Multiphysics. We first designed a full mesa structure for an LED consisting of *p*-GaN/MQWs/*n*-GaN/un-doped GaN/sapphire substrate. Based on the mesa structure, we added ITO, GR, and RAM 150 CSL and made a *p*-metal pad on each CSL and an *n*-metal pad on *n*-GaN. To obtain the proper contact resistance values in the simulation, we have brought varieties to the contact resistance values in order to minimize the differences between the measured current and the simulated current at the 20 mA conditions. The obtained contact resistance values were 3.4×10^{-2} $\Omega\cdot cm^2$, 1×10^{-1} $\Omega\cdot cm^2$ and 5.7×10^{-2} $\Omega\cdot cm^2$ for ITO, GR and RAM 150 CSL, respectively. Moreover, the conductivity values of the ITO, Ag, and graphene sheet were obtained from the aforementioned measurements, the results of which are shown in Fig. 2. As can be seen in Fig. 6, the lateral current using GR CSL was almost confined near the p- type metal pad due to the high sheet resistance value. In contrast, the lateral current using ITO CSL was more widely distributed from the *p*- metal pad due to the moderately low sheet resistance value. Compared to those of the GR and ITO CSLs, however, the lateral current distribution using RAM CSL was totally different. In RAM CSL, the current laterally flows along the metal lines and spreads through the graphene sheet regardless of how far the *p*-metal pad extends. Thus, in the case of RAM 150 CSL, the higher surface charge density

due to the addition of Ag mesh becomes a new source of current flow and the current flow can be distributed widely by adding a two-dimensional graphene sheet. The simulation results strongly agreed with our experimental results and the origin of the better current spreading with metal meshes becomes much more comprehensible.

4. Conclusion

In conclusion, we have fabricated Ag-mesh-combined graphene CSLs for GaN-based NUV LEDs having three different sizes of gap between the mesh lines: 300 μm, 150 μm, and 75 μm. In order to examine the suitability of these materials as CSLs, the electrical and optical properties of the Ag-mesh-combined graphene sheet were investigated using Hall measurement, Raman spectroscopy, and UV-vis-NIR spectrometry. The Ag-mesh-combined graphene sheet with 150 μm gap (RAM 150) showed the most suitable properties for a CSL, with a value of 2.3 Ω/□ for sheet resistance and a value of 86.2 % for transmittance. As a result, the light output power of the NUV LEDs with RAM 150 was the highest at both the same current injection and at the same input power. This was possible due to the lowering of the sheet resistance via the adoption of an Ag mesh and the networking of the Ag mesh using a graphene sheet with very little transmittance loss. Thus, it was confirmed that metal-mesh-combined graphene is suitable for use as a CSL in LEDs, especially in NUV LEDs, in which ITO cannot be used as a CSL.

Acknowledgments

This research was supported by the Core Technology Development Program for Next-generation Energy of Research Institute for Solar and Sustainable Energies (RISE), GIST and this research was supported by Basic Science Research Program through the National Research Foundation of Korea (NRF) funded by the Ministry of Education (NRF-2013R1A1A2A10006632).

References

1. H. Kudo, M. Sawai, Y. Suzuki, X. Wang, T. Gessei, D. Takahashi, T. Arakawa, and K. Mitsubayashi, Sens. Actuator B-Chem., 2010, 147, 676–680.

2. N. G. Jablonski and G. Chaplin, Proc. Natl. Acad. Sci. U. S. A., 2010, 107, 8962–8968.

3. S. J. Gwak, P. Arunkumar, and W. B. Im, J. Phys. Chem. C, 2014, 118, 2686–2692.

4. X. Guo and E. F. Schubert, Appl. Phys. Lett., 2001, 78, 3337.

5. V. K. Malyutenko, S. S. Bolgov, and A. D. Podoltsev, Appl. Phys. Lett., 2010, 97, 251110.

6. S. Nakamura, T. Mukai, and M. Senoh, Appl. Phys. Lett., 1994, 64, 1687.

7. S. Niki, M. Contreras, I. Repins, M. Powalla, K. Kushiya, S. Ishizuka, and K. Matsubara, Prog. Photovolt., 2010, 18, 453–466.

8. G. Jo, M. Choe, C. Y. Cho, J. H. Kim, W. Park, S. Lee, W. K. Hong, T. W. Kim, S. J. Park, B. H. Hong, Y. H. Kahng, and T. Lee, Nanotechnology, 2010, 21, 175201.

9. Z. Li, J. Kang, Z. Liu, C. Du, X. Lee, X. Li, L. Wang, X. Yi, H. Zhu, and G. Wang, AIP ADVANCES, 2013, 3, 042134.

10. T. Kim, A. Canlier, G. H. Kim, J. Choi, M. Park, and S. M. Han, ACS Appl. Mater. Interfaces, 2013, 5, 788–794.

11. J. M. Lee, H. Y. Jeong, K. J. Choi, and W. I. Park, Appl. Phys. Lett., 2011, 99, 041115.

12. J. –P. Shim, T. H. Seo, J. –H. Min, C. M. Kang, E. –K. Suh, and D. –S. Lee, Appl. Phys. Lett., 2013, 102, 151115.

13. S. G. Zhang, X. W. Zhang, F. T. Si, J. J. Dong, J. X. Wang, X. Liu, Z. G. Yin, and H. L. Gao, Appl. Phys. Lett., 2012, 101, 121104.

14. A. H. Castro Neto, F. Guinea, N. M. R. Peres, K. S. Novoselov, and A. K. Geim, Rev. Mod. Phys., 2009, 81, 109.

15. X. Li, W. Cai, J. An, S. Kim, J. Nah, D. Yang, R. Piner, A. Velamakanni, I. Jung, E. Tutuc, S. K. Banerjee, L. Colombo, and R. S. Ruoff, Science, 2009, 324, 1312.

16. K. S. Kim, Y. Zhao, H. Jang, S. Y. Lee, J. M. Kim, K. S. Kim, J. H. Ahn, P. Kim, J. Y. Choi, and B. H. Hong, Nature, 2009, 457, 706.

17. N. Balasubramanian and A. Subrahmanyam, J. Phys. D-Appl. Phys., 1989, 22, 206–209.

18. B. J. Kim, C. Lee, Y. Jung, K. H. Baik, M. A. Mastro, J. K. Hite, C. R. Eddy, Jr., and J. Kim, Appl. Phys. Lett., 2011, 99, 143101.

19. J. –H. Min, M. Son, S. –Y. Bae, J. –Y. Lee, J. Yun, M. –J. Maeng, D. –G. Kwon, Y. Park, J. –I. Shim, M. –H. Ham, and D. –S. Lee, Opt. Express, 2014, 22, 1040.

20. K. –H. Lee, S. –M. Kim, H. Jeong, Y. Pak, H. Song, J. Park, K. –H. Lim, J. –H. Kim, Y. S. Kim, H. C. Ko, I. K. Kwon, and G. –Y. Jung, Adv. Mater., 2013, 25, 3209–3214.

21. J. H. Park, D. Y. Lee, Y. –H Kim, J. K. Kim, J. H. Lee, J. H. Park, T. –W Lee, and J. H. Cho, ACS Appl. Mater. Interfaces, 2014, 6, 12380–12387.

22. H. –J Kim, S. –H. Lee, J. Lee, E. –S. Lee, J. –H. Choi, J. –H. Jung, J. –Y. Jung, and

D. –G. Choi, Small, 2014, 10, 3767–3774.

23. I. N. Kholmanov, C. W. Magnuson, A. E. Aliev, H. Li, B. Zhang, J. W. Suk, L. L. Zhang, E. Peng, S. H. Mousavi, A. B. Khanikaev, R. Piner, G. Shvets, and R. S. Ruoff, Nano Lett., 2012, 12, 5679–5683.

24. L. Wang, W. Liu, Y. Zhang, Z. –H. Zhang, S. T. Tan, X. Yi, G. Wang, X. Sun, H. Zhu, and H. V. Demir, Nano Energy, 2015, 12, 419–436.

25. Y. Zhu, Z. Sun, Z. Yan, Z. Jin, and J. M. Tour, ACS nano, 2011, 5, 6472–6479.

26. H. –J. Shin, W. M. Choi, D. Choi, G. H. Han, S. –M. Yoon, H. –K. Park, S. –W. Kim, Y. W. Jin, S. Y. Lee, J. M. Kim, J. –Y Choi, and Y. H. Lee, J. Am. Chem. Soc., 2010, 132, 15603.

Figures

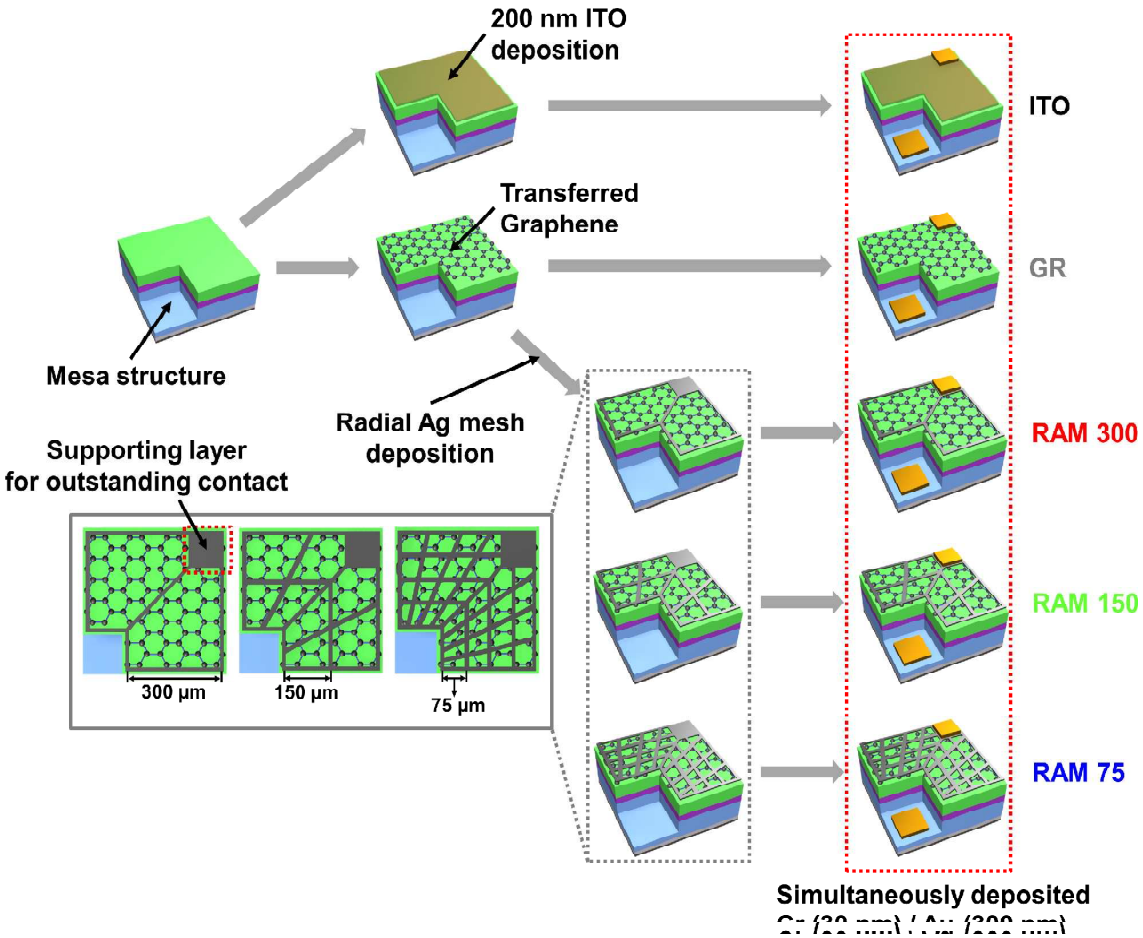

Fig. 1. Process of fabricating the NUV LEDs with different current spreading layers: 200 nm-thick ITO (ITO), graphene (GR), 300 μm-gap radial Ag mesh on graphene (RAM 300), 150 μm-gap radial Ag mesh on graphene (RAM 150), and 75 μm-gap radial Ag mesh on graphene (RAM 75). The inset at the bottom left box is a top view of the NUV LEDs fabricated using radial Ag mesh with a graphene sheet having three different types of gap.

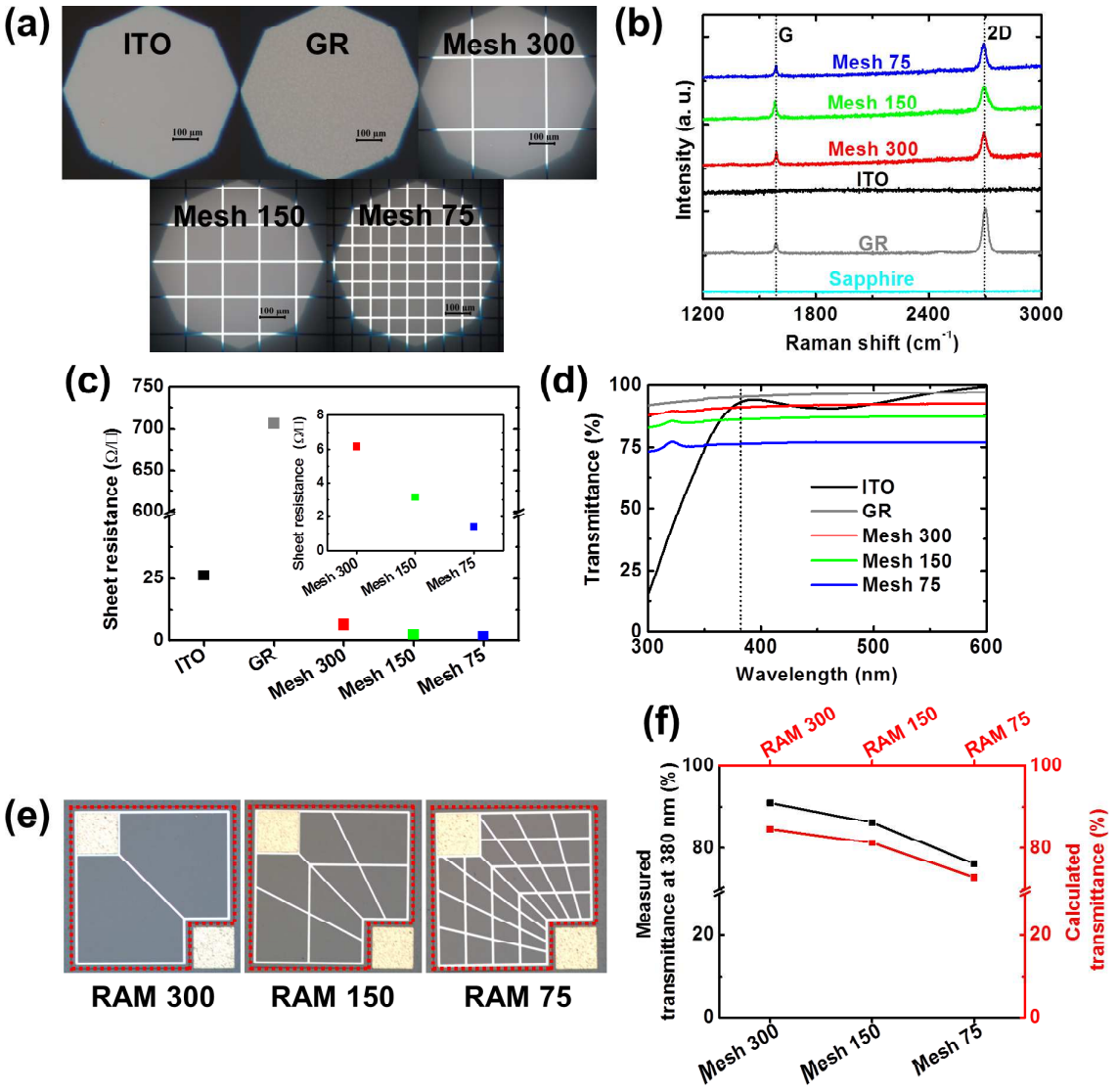

Fig. 2. (a) Optical microscope images of ITO, GR, 300 μm-gap Ag mesh on graphene (Mesh 300), 150 μm-gap Ag mesh on graphene (Mesh 150), and 75 μm-gap Ag mesh on graphene (Mesh 75). (b) Results of Raman spectroscopy with respect to GR, ITO, Mesh 300, Mesh 150, Mesh 75, and sapphire as a reference. (c) Sheet resistances of each material obtained by Hall measurements. The inset represents the sheet resistances in detail of Ag mesh with a graphene sheet. (d) Transmittance of each material. (e) Optical microscope images of the fully fabricated NUV LEDs. (f) Measured transmittances of Mesh 300, Mesh 150, and Mesh 75 at 380 nm, and calculated transmittances of RAM 300, RAM 150, and RAM 75.

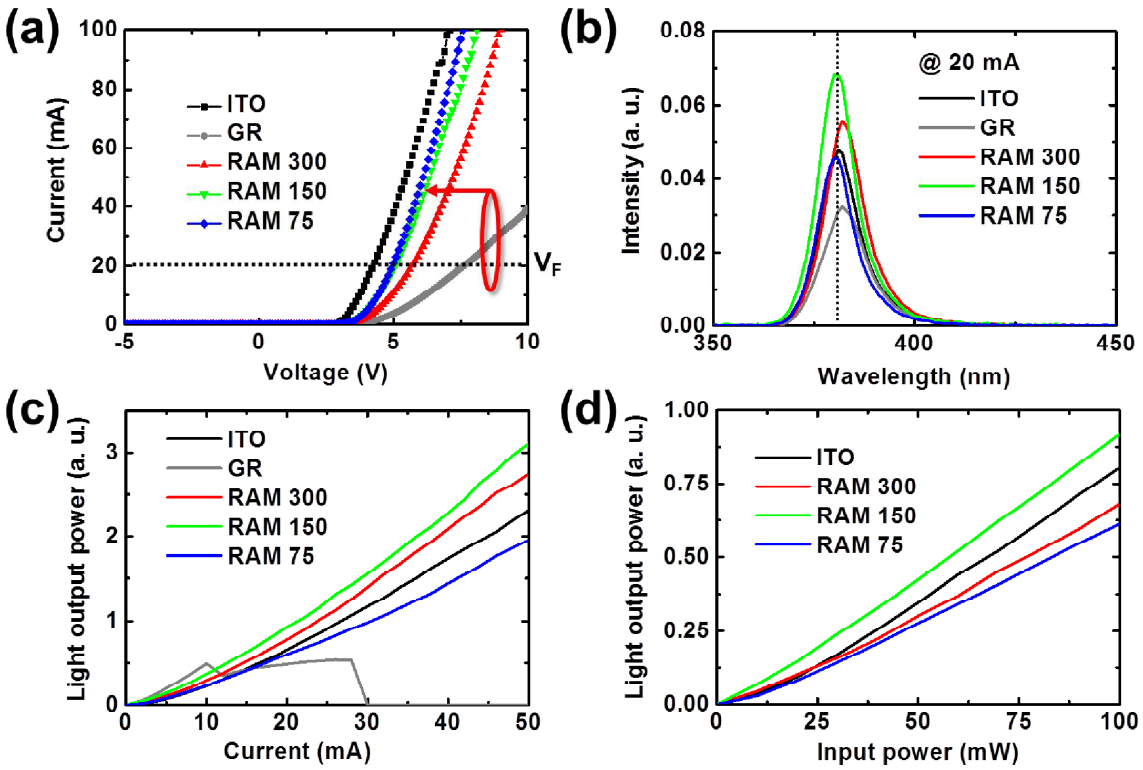

Fig. 3. (a) Current-voltage characteristics of ITO, GR, RAM 300, RAM 150, and RAM 75. (b) Electroluminescence spectra at 20 mA. (c) Light output power versus input current. (d) Light output power versus input power.

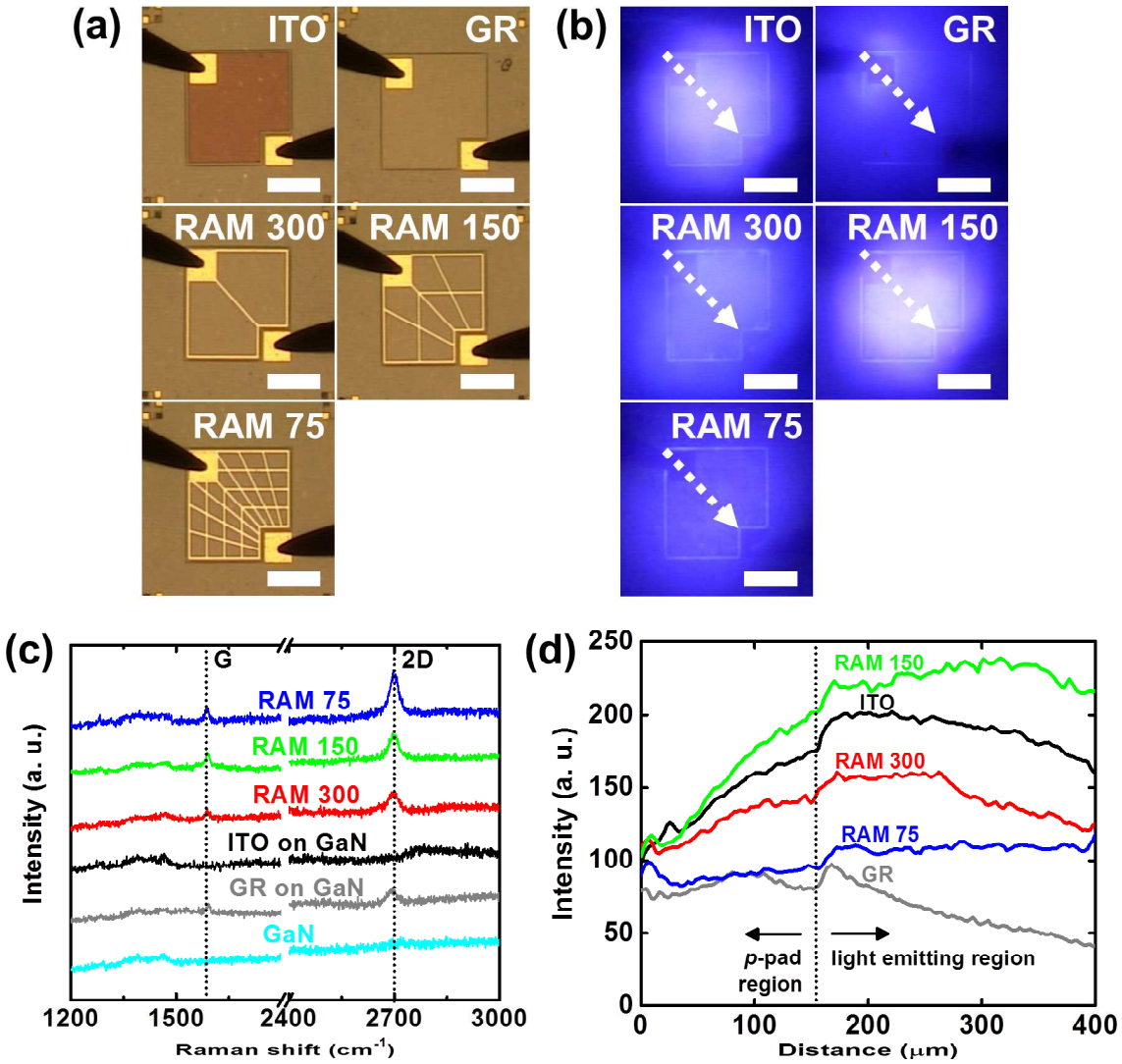

Fig. 4. (a) Optical microscope images of each device before current injection. Scale bar is 200 μm. (b) Optical microscope images of each device after 20 mA injection. Scale bar is 200 μm. (c) Results of Raman spectroscopy with respect to GR, ITO, RAM 300, RAM 150, RAM 75, and GaN as a reference. (d) Luminous intensity of each device versus distance between p-pad and n-pad, marked by white-dot arrows in (b).

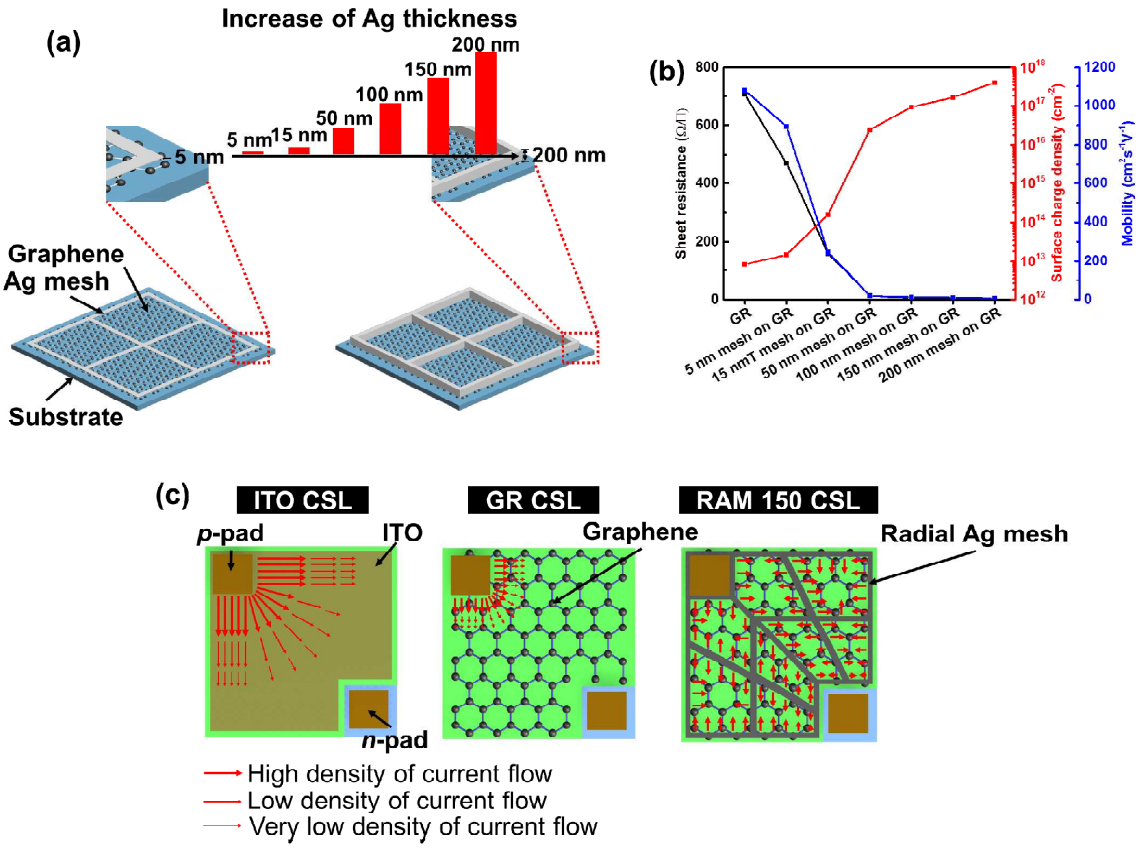

Fig. 5. (a) Schematic of Ag-mesh-combined graphene CSL on DPS with the increase of Ag thickness. (b) Results of Hall measurements related to sheet resistance, surface charge density, and mobility. (c) Lateral current flow through ITO, GR, and RAM 150 CSL.

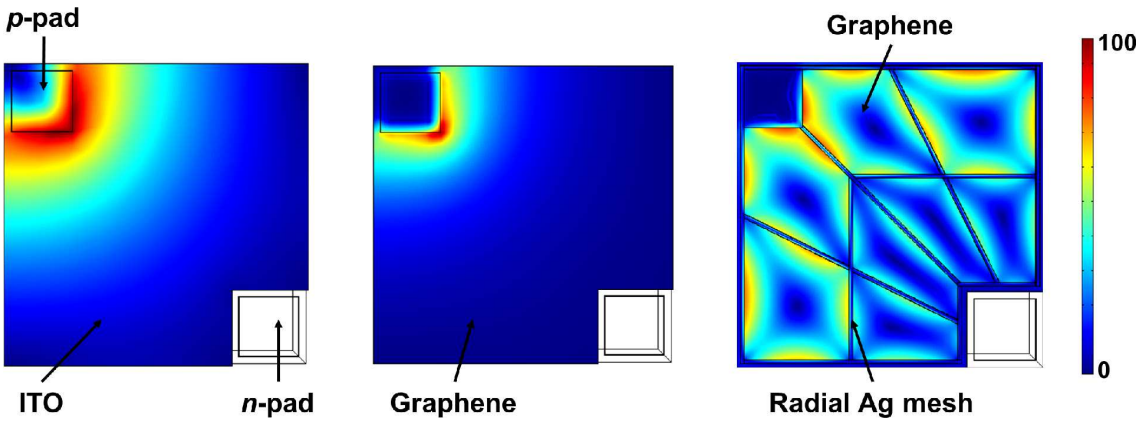

Fig. 6. Simulation results for current flow using ITO, GR, and RAM 150 CSL.

TOC

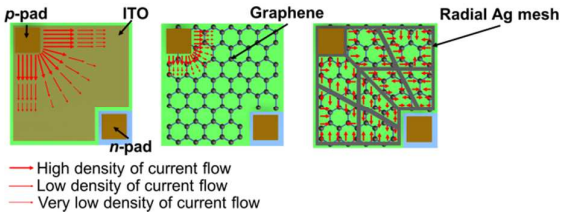

Current spreading could be improved by using Ag-mesh-combined graphene sheets due to dramatically reducing the sheet resistance.